Micro-photoluminescence characterisation of structural disorder in resonant tunneling diodes for THz applications

M. Cito[a], R.Baba[a], D. Childs[a], B. A. Harrison[b], A. Watt[b], T. Mukai[c], and R.A. Hogg[a]
[a] James Watt School of Engineering, University of Glasgow, Oakfield Avenue, G12 8LT Glasgow, United Kingdom
[b]EPSRC National Centre for III-V Technologies, Department of Electronic & Electrical Engineering, University of Sheffield, North Campus, Broad Lane, Sheffield S37HQ, United Kingdom
[c]Sensing Technology R&D Project, R&D Headquarters LED Division, ROHM Co. Ltd., 21 Saiin Mizosaki-cho, Ukyo-ku, Kyoto 615-8585, Japan

ABSTRACT

We investigated the difference between a macro scale PL and μPL (excitation and detection area ≤ 5μm^2). Low-temperature micro-photoluminescence (μPL) is used to evaluate structural perfection of high current density InGaAs/AlAs/InP resonant tunnelling diodes (RTD) structure on different length scales. The thin and highly strained quantum wells (QWs) is subject to monolayer fluctuations in well and barrier thickness that can lead to random fluctuations in their band profile. μPL is performed reducing the laser spot size using a common photolithography mask to reach typical RTD mesa size (a few square microns). We observed that for spot size around 1μm^2 the PL line shape present strong differences on multiple points on the wafer. These variations in the PL is investigated by line-shape fitting and discussed in terms of variations in long-range disorder brought about by strain relaxation processes. We also highlight this μPL as a powerful and cost-effective non-destructive characterization method for RTD structures.

Keywords: photoluminescence spectroscopy, resonant tunnelling diodes, THz

1. INTRODUCTION

We previously demonstrated how the RTD undesired valley current is not only limited by thermal effects but mainly by heterointerface scattering [1], with only ~20% of the valley current being thermally activated, leaving space for improvement of the crystal quality. To optimize the epitaxial process, luminescence techniques are appealing for their ability to characterize epitaxial wafers electrically and physically. We initially demonstrated the use of PL as a rapid non-destructive characterization technique [2] to evaluate the doping profile and the QW characteristics. Further work demonstrated a non-destructive characterization scheme based on low-temperature photoluminescence spectroscopy (PL) in combination with high-resolution X-ray diffraction (HD-XRD), improved by the inclusion of a buried undoped "copy" QW [3]
Additional improvement on the repeatability of the epitaxial structure has been obtained by applying photoluminescence excitation spectroscopy (PLE), used to deduce critical information on the band offset [4]
Comparison with TEM underlined how critical structural parameters can be derived from this non-destructive post-growth characterization scheme [5].

In this paper, we demonstrate the use of PL to evaluate the wafer uniformity in one high current density RTD design with QW under high strain conditions. We progressively increased the spatial resolution reducing the PL laser spot-size, reaching the typical RTD mesa-size of few square microns. This reduction is obtained by employing circular windows (holes) of reducing area on a photolithography mask mounted on the top of the sample. We observed strong PL line shape differences associated with short- and long-range structural disorders originated by strain stress in the QW.

Structures were grown using a Thomas Swan 7x2 robot-loaded close-coupled showerhead (CCS), metal-organic vapour phase (MOVPE) reactor. The group III precursors were trimethylalluminium (TMA), trimethylgallium (TMG) and

trimethylindium (TMI), whilst the group V precursors were arsine (AsH_3) and phosphine (PH_3). A 300nm InP buffer was deposited at 580°C on Fe doped InP (001) offcut by 0.1 degrees towards (111). The rest of the structures were grown at 595°C. 200nm of AlInAs was grown to getter oxygen and improve the AlAs barrier symmetry, whilst 25nm of InGaAs was grown to aid the nucleation of the AlInAs. A CP21 wet etch profiler and Hall measurements were used to calibrate the doping concentrations and the layer compositions were calibrated using a Bruker D8 Discovery.

After the InP buffer, the overgrowth continues with 200 nm undoped $In_{0.53}Ga_{0.47}As$. 400 nm highly n-doped $In_{0.53}Ga_{0.47}As$ ($2x10^{19}$ cm^{-3} Si) is then grown for the lower contact. A 20 nm n-doped $In_{0.53}Ga_{0.47}As$ ($3x10^{18}$ cm^{-3} Si) emitter layer is then deposited, followed by a 2 nm $In_{0.53}Ga_{0.47}As$ spacer layer. 16MLs (4.7nm) of $In_{0.8}Ga_{0.2}As$ quantum well is formed between two 1.1 nm AlAs barriers. On the collector side, a 20 nm $In_{0.53}Ga_{0.47}As$ spacer layer is grown with a 25 nm $In_{0.53}Ga_{0.47}As$ ($3x10^{18}$ cm^{-3} Si) collector layer. The epitaxy is terminated with 15 nm n-doped $In_{0.53}Ga_{0.47}As$ ($2x10^{19}$ cm^{-3} Si), and 8 nm $In_{0.80}Ga_{0.20}As$ ($2x10^{19}$ cm^{-3} Si).

2. MONO-LAYER FLUCTUATION

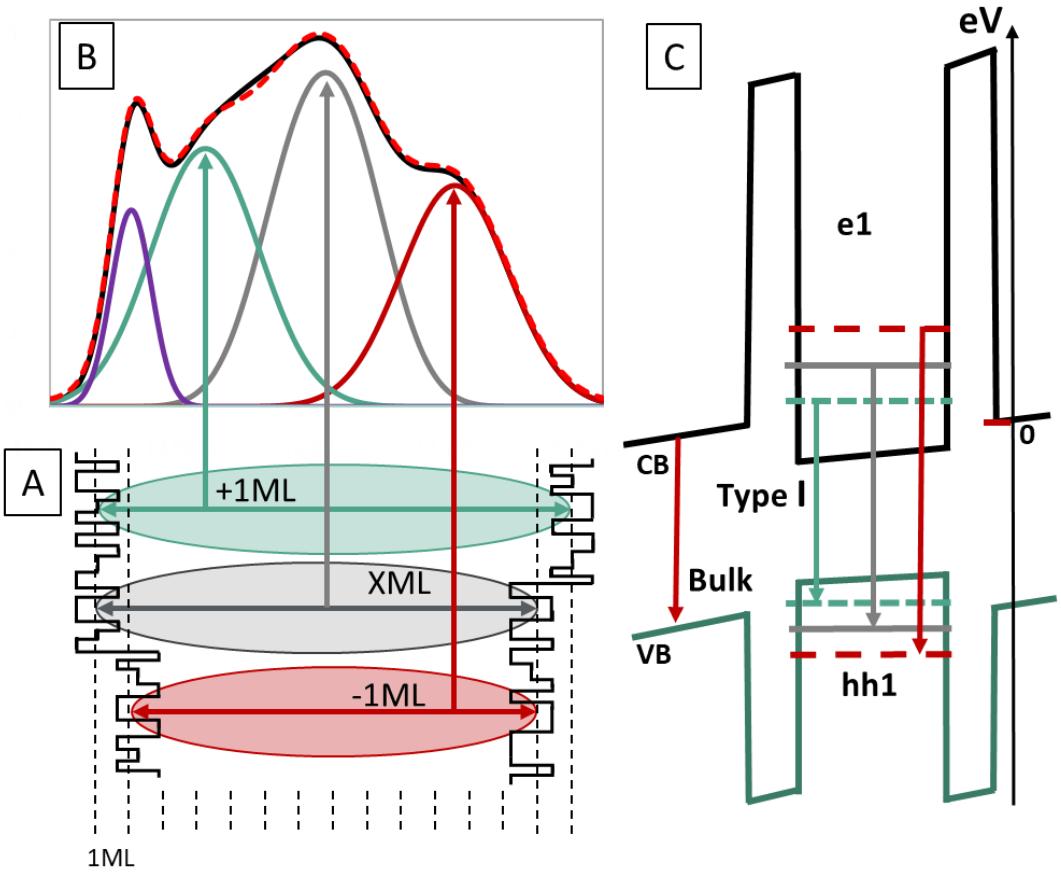

Figure 1 (A) schematic micrograph describing the heterointerface roughness(vertical black line) and the mono-layer fluctuation in the QW thickness (Vertical black dashed lines). Coloured horizontal arrows are indicating the ML thickness, ovals are indicating the exciton radius (see text). (B) Representative PL spectra and peaks deconvolution. (C) Band profile and QW Type Radiative transitions, X ML (grey), -1ML (Red) and +1ML (green).

The group of schematics and micrographs reported in figure1 are intended to illustrate the mono-layer fluctuations present within our samples at the heterointerfaces and their impact on the PL characterization.

Picture 1(A) is a 1D schematic and not an in-scale representation of the imperfection associated with the QW growth process. Black lines are highlighting the roughness at the AlAs/InGaAs heterointerfaces. Black dashed vertical lines are indicating the QW thickness, expressed in ML units. Coloured lines are indicating the ML fluctuation that characterizes the QW, designed thickness in grey (X ML), plus 1ML in green (+ 1ML) and minus 1ML in red (-1ML). The coloured ellipses are representing the electron-holes excitons, with a radius of 10nm they act as a probe to measure and discriminate between long-range (length scale>>exciton) and short-range (length scale<<exciton) structural disorders.

Figure 1(B) shows a typical low-temperature PL spectrum: the barrier roughness (short-range disorder) creates broad PL peaks while the ML-fluctuation (long-range disorder) cause peak splitting and an overall broadening of the PL trace [6]. Figure 1(C) shows a schematic representation of the RTD active region band profile and the radiative transitions detectable by PL. The conduction band is reported in black, while the valence band in dark green. Following the same colour scheme from the previous pictures, horizontal lines are highlighting the QW first quasi-bound states e1 (hh1). The PL optical transitions are indicated by vertical lines, the type 1 transition goes from e1 to hh1 while the bulk transition is associated with the LM-InGaAs band-gap. Fiure1(C) clarified numerically the origin of the peak splitting described in figure 1(b): the ML-fluctuation creates 2 additional quasi-bound states (±1ML) in addition to the designed one (XML), the type I transition is now a triplet [6].

Scanning Cathodoluminescence (CL) study on the GaAs/AlGaAs material system demonstrated for the first time that the in-plane extension of these ML fluctuations, the 3D nucleation generates ML regions known as "ML island islands" with an area >2μm^2 [7]. For the InGaAs/InP material system under high strain conditions ([In] ≥ 80%), similar results were observed by atomic force microscopy (AFM) [8] and scanning tunnelling microscopy (STM) [9].

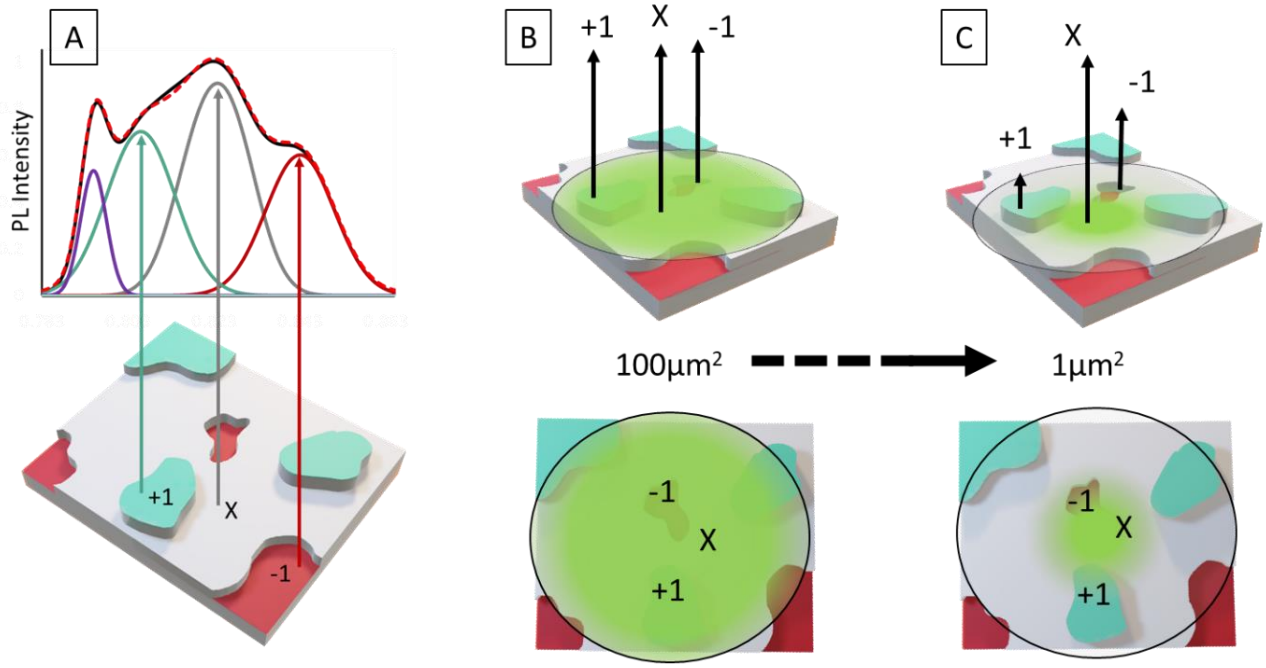

Figure 2 (A) ML island schematization on effect on the PL spectra. (B-C) Area and ML island covered by a broad and a thin PL laser spot size. ML island indicated by numbers.

Starting from the left, the bottom of Figure 2(A) describes the ML fluctuation with a 3D-pictogram and highlights the random shape and the in-plane extension of the ML island. The grey surface represents the designed XML thickness while the coloured zones are the ±1ML islands. Similar to figure1(A), the top of figure 2(B) describes the correlation between the ML island and the PL peaks. Figure 2(B) describes how the PL laser illuminates the sample, the broad spot-

size excite all the ML island, and the collected PL spectra give spatial-averaged information about the wafer electrical properties. Figure 2(C) show that a thin spot size can be used to reduce background emissions and maybe excite a single ML island.

Typical RTD mesa sizes vary with application, ranging from 25μm^2 for Sub-THz oscillators [10] to ~1um^2 for high Jpeak structures for THz operation [11, 12]. Such device/mesa dimensions are comparable with the expected extension of these ML-islands.

3. PHOTOLUMINESCENCE SPECTROSCOPY

Low-temperature PL was performed in a closed-cycle helium cryostat, with the sample at a temperature of 13K. A frequency-doubled neodymium-doped yttrium-vanadium-oxide (Nd:YVO4) laser at 532 nm was used to excite the sample. The PL signal was filtered by a double-grating Bentham DMc150 monochromator and detected by an InGaAs transimpedance photodetector. Measurements were conducted using a laser power density of ~0.5 mW/cm^2. PL is performed at low-temperature to suppress the non-radiative process and enhance the radiative ones, improving the linewidth and so the spectroscopy details [13]. As described by the micrograph in figure 2, we need to move from a macro-scale PL (figure 2B) to a micro-scale PL (figure 2C), to this end, we employed a photolithography mask to reduce the laser spot size.

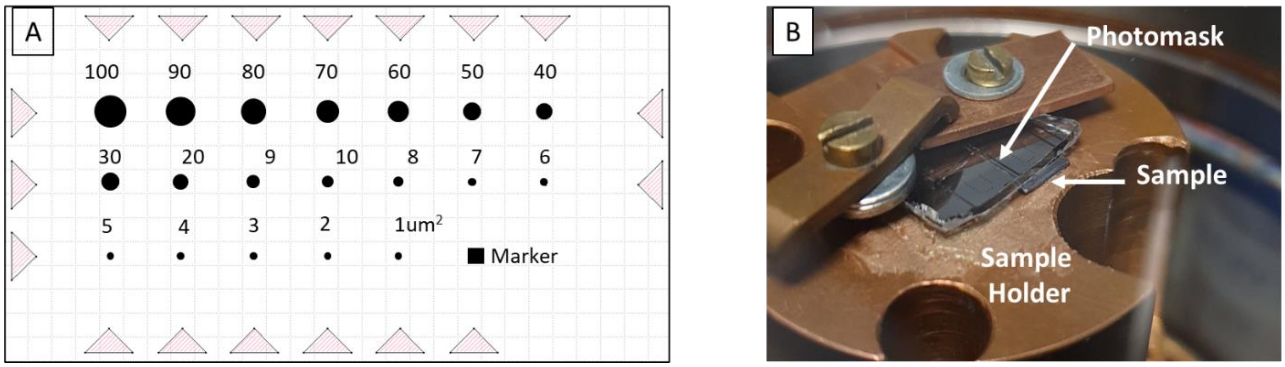

Figure 3 (A) photomask pattern design, numbers are indicating the area dimension. (B) Measurement set-up, from the top: Copper blocking system, photomask, sample, and copper sample holder.

Figure 3(A) shows the photomask design that covers an area lower than 1 cm^2. The designed pattern has 19 different holes, with dimensions providing areas from 100 μm^2 to 10 μm^2 (step of 10 μm^2) and from 9 μm^2 to 1 μm^2 (step of 1 μm^2). The mask is a common commercial 3"x3"x0.006" chrome/quarts photolithography mask, positioned with the chrome absorber in contact with the sample. Each hole is surrounded by triangular markers to help the alignment of the PL laser. Each element of the pattern is separated by 300μm to eliminate possible contribution from the surrounding windows. Figure 3(B) is a photograph of the experimental setup. From the top we observe the photolithography mask pressed on the wafer sample using copper plates as a blocking system. The sample holder is covered in vacuum grease to improve the thermal bonding.

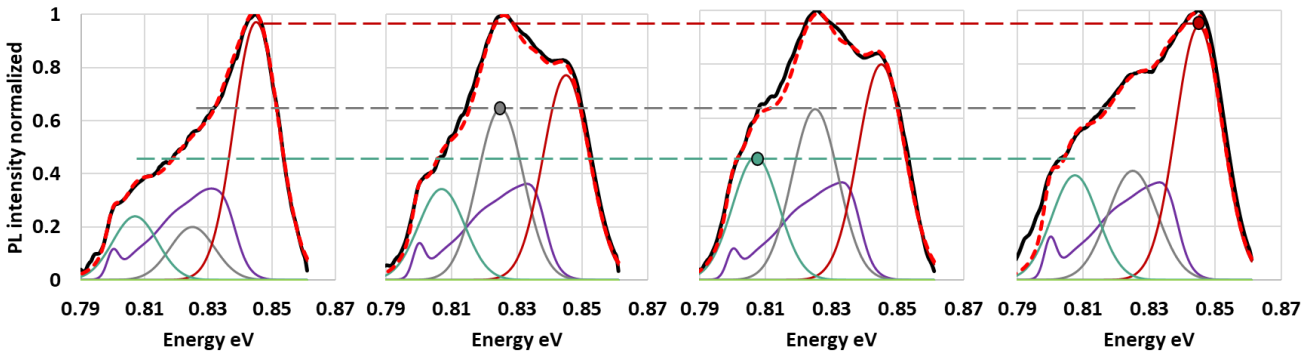

Figure 4 Micro-PL spectra (Black) and line shape fitting (red dashed line) from 4 different parts of the wafer with a spot size of 1μm^2 . Purple curve indicates the Bulk peak.

We observed PL line shape differences reducing the window area, and the strongest differences are detected by window areas lower than 5 μm^2. On this basis, we focused the attention on the 1 μm^2 window to scan 4 different sections of the wafer, results are reported in the micrographs in figure 4. Measured PL spectra are reported in black, and each micrograph shows a different line shape, highlighting differences around the sample. We previously demonstrated how the PL line-shape fitting can be used to provide more information from the PL spectra, especially in the case of strong peak overlapping like the one presented here.

The line shape fitting is based on several constraints to regulate the position, shape, and amplitude of the peaks. The deconvolution of the Type I emission is obtained using 3 Gaussian peaks (μ, σT1) (X ML, ±1 ML). Their position on the energy axis (μ) is based on simulation made using the model-solid theory. We assume an equal linewidth (σT1) for the three Type I transitions [3].

Fitting results are indicated by dashed red lines, purple lines are indicating the doped InGaAs and the bulk LM-InGaAs, the type-I components are indicated in red (-1ML), in grey (XML), and in green (-1). Accordingly with our simulation, the XML peak is positioned at 0.825eV, the +1ML at 0.799eV and the -1ML at 0.843eV. The fitting is obtained using Gaussian peak with a used σT1=7 meV for the type I transitions. The bulk peak has a linewidth of 4meV, in agreement with the limit of 3.3meV predicted for perfect LM-InGaAs [14].
All four line-shape fittings are obtained fixing the position and the variance of each peak and varying only their amplitude. The Peak intensity strongly differs in some graphs, the maximum intensity reached by each transition is highlighted by coloured dots and compared with the other micrograph by the horizontal lines. As no tuning in σT1 was needed for the line shape fitting, we can assume that the short-range disorder attributed to the heterointerface roughness is constant around the wafer or has fluctuation in a range scale not detectable by the micro PL.

The InGaAs QW is grown on the first AlAs barrier, this barrier alone has to balance the QW 16-ML stress until the second barrier is complete, for highly-mismatched design, imperfections are more likely to occur [15, 16]. This thick stack of MLs is more exposed to strain-induced relaxation due to nucleation of dislocation [17] leading to the formation of islands [18, 19]. For the coherent growth of strained structures without the formation of dislocations, the limit has often been described in terms of the *critical thickness*, defined as the maximum achievable thickness of a material X pseudomorphically grown on material Y [20]. The more realistic limit was modelled using a mechanical equilibrium approach by Matthews & Blakeslee (M&B) [21]. This model was investigated for the AlAs/InGaAs/InP material system [22] to design highly-strained QWs and for the optimization of the high-current-density RTD designs.

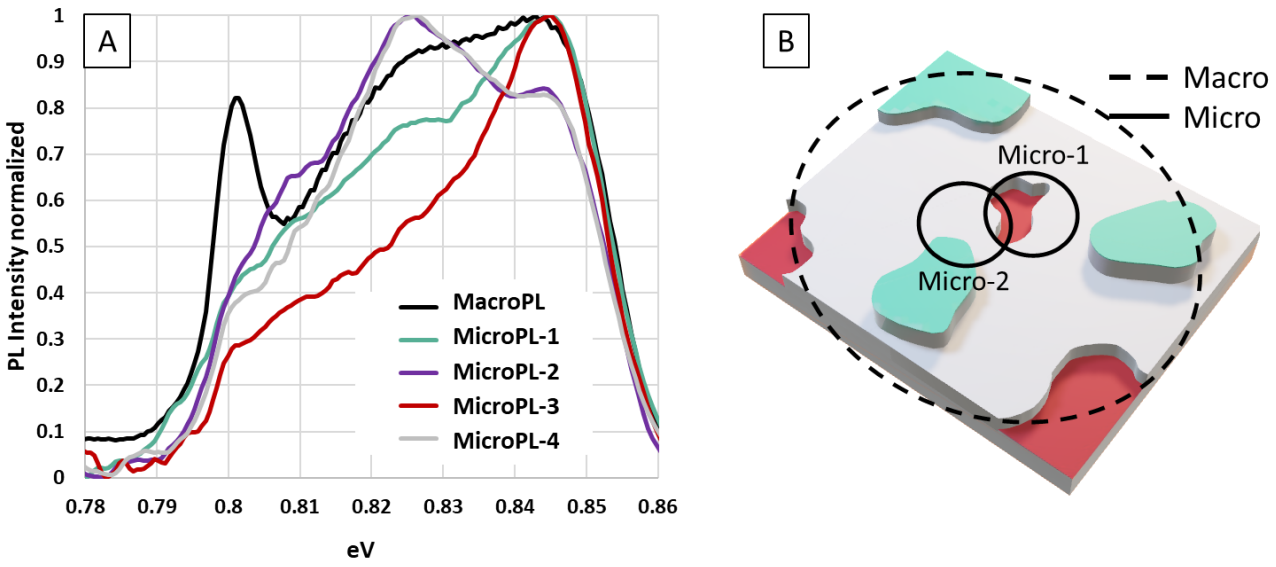

Figure 5 (A) PL comparison between the macro-scale and the 4 micro-scale measurement presented in figure 4. (B) schematic of the MLs covered by a macro spot size (black dashed circle) and 2 representative micro spots (black circles).

Figure 5(A) shows a standard macro scale PL (black line) and the four micro-PL curves presented in figure 4. Data are normalized for comparison. Starting from the lower energy side of the spectra, the bulk peak at 0.8 eV is strong, and at higher energy, the PL intensity is distributed between all the 3 type-I peaks. The Bulk transition is weak in the micro-PL scans and the type I emissions have different intensities, depending on the ML island covered by the laser spot size. Figure5(B) shows a macro spot size, represented by the black dashed line and it is compared with two representative micro spot sizes, (black lines). ML islands are distributed uniformly on the wafer surface and their extension is arbitrary[7]. On this basis, each micro spot may cover multiple ML islands but in different proportions, the resulting spectra are characterized by the ML peak of the most covered island.
As an example, we focus the attention on the red line in figure5(A) (micro), where the spectra is dominated by the -1ML transition at 0.84eV. For this curve we can assume a spot size like the one indicated as micro-1 in figure 5(B), this area covers in great part a -1ML island and its contribution to the PL spectra is the highest.

The data presented are suggesting that a careful interpretation of the PL spectra is needed when QWs are under high strain conditions. The micro PL indicate that the detected average electronics property in a 1μm^2 area may strongly differ from a macro scale and other parts of the same sample.

4. CONCLUSION

We have presented the application of micro-PL to qualitative observe micro-scale non-uniformities of high-J InGaAs/AlAs/InP RTD structures for THz applications, not observable through standard macro-scale PL. The analysed sample has shown to exhibit different long-range disorders through the variation of their PL line shapes with reducing excitation/detection area. Furthermore, device fabrication and characterization may prove a correlation between the observed non-uniformities and their impact on the device performance and reproducibility.

Acknowledgment

This project has received funding from the European Union's Horizon 2020 research and innovation programme under the Marie Skłodowska-Curie grant agreement No 765426 (TeraApps).

REFERENCES

1. Jacobs, K., et al., *Valley current characterization of high current density resonant tunnelling diodes for terahertz-wave applications.* AIP Advances, 2017. **7**(10): p. 105316.
2. Jacobs, K.J., et al. *Characterisation of high current density resonant tunnelling diodes for THz emission using photoluminescence spectroscopy*. in *2016 41st International Conference on Infrared, Millimeter, and Terahertz waves (IRMMW-THz)*. 2016. IEEE.
3. Baba, R., et al., *Non-destructive characterization of thin layer resonant tunneling diodes.* Journal of Applied Physics, 2019. **126**(12): p. 124304.
4. Cito, M., et al., *Photoluminescence excitation spectroscopy for structural and electronic characterization of resonant tunneling diodes for THz applications.* AIP Advances, 2021. **11**(3): p. 035122.
5. Baba, R., et al. *Characterisation of thin-layer resonant tunnelling diodes grown by MOVPE*. in *Quantum Dots and Nanostructures: Growth, Characterization, and Modeling XVI*. 2019. International Society for Optics and Photonics.
6. Cito, M., et al. *Fitting of photoluminescence spectra for structural characterisation of high current density resonant tunnelling diodes for THz applications*. in *Terahertz, RF, Millimeter, and Submillimeter-Wave Technology and Applications XIV*. 2021. International Society for Optics and Photonics.
7. Christen, J., M. Grundmann, and D. Bimberg, *Scanning cathodoluminescence microscopy: A unique approach to atomic-scale characterization of heterointerfaces and imaging of semiconductor inhomogeneities.* Journal of Vacuum Science & Technology B: Microelectronics and Nanometer Structures Processing, Measurement, and Phenomena, 1991. **9**(4): p. 2358-2368.
8. Sugiyama, H., et al., *Metal-organic vapor-phase epitaxy growth of InP-based resonant tunneling diodes with a strained In0. 8Ga0. 2As well and AlAs barriers.* Japanese journal of applied physics, 2005. **44**(10R): p. 7314.
9. Porte, L., *Stress and surface energies versus surface nanostructuring: the InGaAs/InP (0 0 1) epitaxial system.* Journal of crystal growth, 2004. **273**(1-2): p. 136-148.
10. Wang, J., et al. *High performance resonant tunneling diode oscillators for THz applications*. in *2015 IEEE Compound Semiconductor Integrated Circuit Symposium (CSICS)*. 2015. IEEE.
11. Suzuki, S., et al., *Fundamental oscillation of resonant tunneling diodes above 1 THz at room temperature.* Applied Physics Letters, 2010. **97**(24): p. 242102.
12. Jacobs, K., et al., *A dual-pass high current density resonant tunneling diode for terahertz wave applications.* IEEE Electron Device Letters, 2015. **36**(12): p. 1295-1298.
13. Grober, R.D., et al., *Design and implementation of a low temperature near-field scanning optical microscope.* Review of scientific instruments, 1994. **65**(3): p. 626-631.
14. Herman, M., D. Bimberg, and J. Christen, *Heterointerfaces in quantum wells and epitaxial growth processes: Evaluation by luminescence techniques.* Journal of Applied Physics, 1991. **70**(2): p. R1-R52.

15. Ekins-Daukes, N., K. Kawaguchi, and J. Zhang, *Strain-balanced criteria for multiple quantum well structures and its signature in X-ray rocking curves.* Crystal Growth & Design, 2002. **2**(4): p. 287-292.
16. Tu, Y. and J. Tersoff, *Origin of apparent critical thickness for island formation in heteroepitaxy.* Physical review letters, 2004. **93**(21): p. 216101.
17. Tersoff, J. and F. LeGoues, *Competing relaxation mechanisms in strained layers.* Physical review letters, 1994. **72**(22): p. 3570.
18. Eaglesham, D. and M. Cerullo, *Dislocation-free stranski-krastanow growth of Ge on Si (100).* Physical review letters, 1990. **64**(16): p. 1943.
19. Nabetani, Y., et al., *Island formation of InAs grown on GaAs.* Journal of crystal growth, 1995. **146**(1-4): p. 363-367.
20. Jain, S., M. Willander, and H. Maes, *Stresses and strains in epilayers, stripes and quantum structures of III-V compound semiconductors.* Semiconductor science and technology, 1996. **11**(5): p. 641.
21. Matthews, J. and A. Blakeslee, *Defects in epitaxial multilayers: I. Misfit dislocations.* Journal of Crystal growth, 1974. **27**: p. 118-125.
22. Baba, R., et al., *Epitaxial Designs for Maximizing Efficiency in Resonant Tunneling Diode Based Terahertz Emitters.* IEEE Journal of Quantum Electronics, 2018. **54**(2): p. 1-11.